Twist-Induced Snapping in a Bent Elastic Rod and Ribbon

Tomohiko G. Sano[1,2,*] and Hirofumi Wada[1,†]
[1]*Department of Physical Sciences, Ritsumeikan University, Kusatsu, Shiga 525-8577, Japan*
[2]*Research Organization of Science and Technology, Ritsumeikan University, Kusatsu, Shiga 525-8577, Japan*

(Received 24 May 2018; revised manuscript received 12 January 2019; published 22 March 2019)

Snapping of a slender structure is utilized in a wide range of natural and manmade systems, mostly to achieve rapid movement without relying on musclelike elements. Although several mechanisms for elastic energy storage and rapid release have been studied in detail, a general understanding of the approach to design such a kinetic system is a key challenge in mechanics. Here we study a twist-driven buckling and fast flip dynamics of a geometrically constrained ribbon by combining experiments, numerical simulations, and an analytical theory. We identify two distinct types of shape transitions: A narrow ribbon snaps, and a wide ribbon forms a pair of localized helices. We construct a phase diagram and explain the origin of the boundary, which is determined largely by the geometry. We quantify the effects of gravity and clarify the timescale dictating the rapid flipping. Our study reveals the unique role of geometric twist-bend coupling in the fast dynamics of a thin constrained structure, which has implications for a wide range of biophysical and applied physical problems.

DOI: 10.1103/PhysRevLett.122.114301

Transforming elastic potential energy to kinetic energy is a key design problem in a range of biological and manmade systems. Elastic instabilities such as buckling, cavitation, and fracture have provided elegant solutions such as those found in plants and fungi [1–5], as well as in a variety of applications including ancient catapults, children's toys, smart materials, and robotics [6–20].

In this study, we reveal the mechanism by which the elastic energy of an anisotropic rod is stored and rapidly released by geometric twist-bend coupling. The illustration of this phenomenon is easy. Take a strip of paper, and hold the two ends so that it forms an arc [Fig. 1(a)]. As the two ends are rotated in the same direction, the ribbon initially deflects, then recoils, and eventually flips with a snap to go back to its previous configuration [Figs. 1(b) and 1(c)]. See Supplemental Material for Video S1 [21]. This simple "clicky" process provides a basis to achieve a cyclic snapping motion that requires no additional recovery or sensory processes, which is a distinct advantage for numerous applications [30–32]. Combining the experiments, simulations, and theory, we show that a narrow ribbon snaps, whereas a wide ribbon forms a pair of localized helices [Fig. 1(d)]. In addition, we identify a geometric criterion for the snapping to occur. The importance of geometric twist-bend coupling has previously been

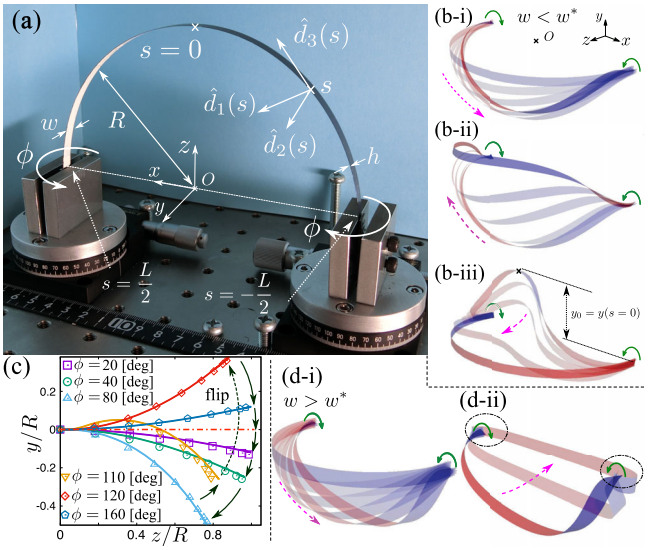

FIG. 1. (a) Geometry of experiments and definition of our coordinate system. Two ends of a ribbon ($s=\pm L/2$) are clamped with controlled twisting angles ϕ. (b-i)–(b-iii) Stroboscopic figures of a flipping ribbon obtained from our numerical simulation for $(h,w,R)=(0.2,8,115)$ mm. The head of the ribbon (b–i) goes down, (b-ii) goes up, and (b-iii) flips. (c) Side view of ribbon center lines obtained in our simulation (solid lines) and experiment (data points) for various ϕ and $(h,w,R)=(0.2,8,108)$ mm. The chain line $y=0$ represents a shape without twist: $\phi=0°$ and 180°. (d-i),(d-ii) Stroboscopic figures of a folding ribbon observed in our simulation for $(h,w,R)=(0.2,15,115)$ mm. Its head (d-i) goes down and (d-ii) raises to the back. The ribbon never flips in this case.

recognized in the study of supercoiling instabilities in biological polymers and fibers [33,34] and the rich morphologies of twisted ribbon [35–38]. Our present study generalizes this concept [39] and shows that it also dictates the statics and dynamics of a slender structure.

We start our investigation with a slender uniform rod, followed by increasing the anisotropy of its cross section, and proceed to a flat ribbon. An intrinsically straight rod or ribbon was mounted on a mechanical system, forming a semicircle of radius R. See Fig. 1(a). The two ends were clamped on rotary optical stages that controlled the rotational angle ϕ. The geometric parameters characterizing a rod configuration are the width w, thickness h, and radius R (related to the arc length L as $L = \pi R$), which are varied in the range of 4–16, 0.12–3.8, and 31–178 mm, respectively. We gradually increased ϕ by carefully rotating the optical stages by hand with an accuracy of 1°. At each step, the system was observed till it attained equilibrium (except in the vicinity of the transition). The morphologies were recorded with a digital camera, and the resulting images are analyzed further below.

To complement the experimental data, we also perform numerical simulations based on the Kirchhoff elastic rod formulation for a narrow ribbon [21–27], where a weak in-plane stretch is taken into account.

A fliplike transition was always observed for a slender anisotropic rod. Only an ideally circular rod ($w/h = 1$) was a singular case, as it would simply rotate axially without any transition. To systematically study the dependence of a critical twisting angle for the transition ϕ^* on the anisotropy, we used silicone-based rods (WAVE, OM143) with different cross-sectional ellipticities [Fig. 2(a)], which were fabricated by curing silicone mixtures inside a radially compressed flexible tube in a controlled manner. To minimize the effects of gravity, which will be detailed later, we used a relatively short rod with $R = 31$ mm for silicone rods, while larger R was employed for stiff metal ribbons. Figure 2(b) shows that the flip angle ϕ^* is nearly 90° for the vanishing anisotropy $w/h \to 1$, while it increases with an increasing w/h and approaches ~115° in the flat ribbon limit $w/h \to \infty$ (as confirmed by our numerical simulations without gravity).

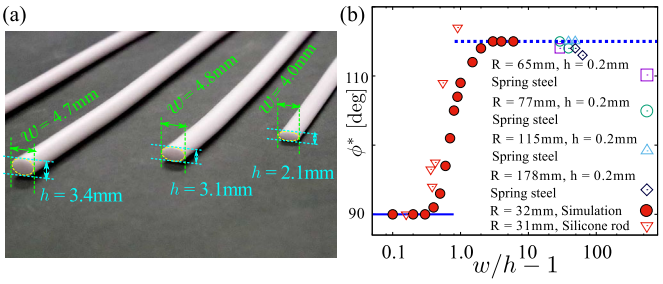

FIG. 2. (a) Image of silicone-based rods with different elliptic cross sections. (b) Flip transition angle ϕ^* as a function of the aspect ratio δ obtained from the simulation and experiment for silicone rods and $h = 0.2$ mm metal ribbon with various R. The dashed and solid lines denote 90° and 115°, respectively.

For a slightly anisotropic rod, we can rationalize the above results by the Kirchhoff rod theory. To describe the ribbon configuration, we assign an orthogonal director frame $(\hat{\boldsymbol{d}}_1, \hat{\boldsymbol{d}}_2, \hat{\boldsymbol{d}}_3)$ at each point of the center line s [Fig. 1(a)]. $\hat{\boldsymbol{d}}_3 = \boldsymbol{r}'$ is the unit tangent vector, where $()'$ denotes the derivative with respect to s, while $\hat{\boldsymbol{d}}_1$ and $\hat{\boldsymbol{d}}_2$ point towards the principal axes in the ribbon's cross-sectional plane [28,29]. Assuming inextensibility, the rod configuration is determined by specifying how the frame rotates as it moves along the center line per unit length: $\hat{\boldsymbol{d}}_a' = \boldsymbol{\Omega} \times \hat{\boldsymbol{d}}_a$ $(a = 1, 2, 3)$, where the direction of $\boldsymbol{\Omega} = \Omega_a \hat{\boldsymbol{d}}_a$ sets the rotational axis at s, and Ω_a gives the rate of rotation, i.e., curvature, about $\hat{\boldsymbol{d}}_a$. Because we consider an almost circular cross section, we quantify its anisotropy by introducing a small expansion parameter $\delta = w/h - 1$. At the lowest order of $\delta \ll 1$, we observe that $\Omega_1 \sim \Omega_2 \sim 1/R$ and $\Omega_3 = O(\delta)$ [21]. Then, the Kirchhoff rod equations are reduced to a set of three independent linear ordinary differential equations: $\Omega_1' = \Omega_2' = 0$ and $\Omega_3' = 2\delta(1+\nu)\Omega_1\Omega_2$. We then construct the solutions for Ω_a, such that the ribbon shape satisfies the boundary conditions at $s = \pm L/2$ and the constraint $\boldsymbol{r}(L/2) - \boldsymbol{r}(-L/2) = 2R\hat{\boldsymbol{x}}$. This leads to $\Omega_1 = \sin\phi/R + O(\delta)$, $\Omega_2 = \cos\phi/R + O(\delta)$, and

$$\Omega_3(s;\phi) = \delta\frac{(1+\nu)s}{R^2}\sin 2\phi + O(\delta^2). \tag{1}$$

The critical angle ϕ^* is known from the condition that the torque applied at the clamped end is zero, $T(\phi^*) \propto \Omega_3(-L/2, \phi^*) = 0$, which predicts $\phi^* = \pi/2 + O(\delta)$.

Having addressed the rod regime, we now focus on the thin flat ribbon to investigate regimes of $w/h \gg 1$. For a small ϕ, a ribbon deflects from the original plane of bending, symmetrically developing left-handed and right-handed helices on each side. With increasing ϕ, we observe two distinctly different behaviors depending on w/h. A relatively narrow ribbon ($w < w^*$) recoils and eventually flips with a snap, returning to its original configuration but now *inside out*; the critical width w^* will be discussed in detail later. Because the helices at the two sides have opposite handedness, they annihilate at the center when they progress, triggering the flip with a snap [Figs. 1(b–i)–1(b-iii)]. In contrast, a sufficiently wide ribbon ($w > w^*$) develops localized helices formed at the proximity of the two ends, which remain separated and stabilized for increasing ϕ [Figs. 1(d-i) and 1(d-ii)]. At self-contact, a further rotation requires the application of an indefinitely large torque, leading to the formation of creases or kinks [40,41]. Hereafter, we refer to this mode as a "fold," and the former as a "flip."

To quantify the three-dimensional shape changes, we tracked the position of a specific point on the ribbon center line at $s = 0$ [see Fig. 1(b-iii)] and plotted its y component,

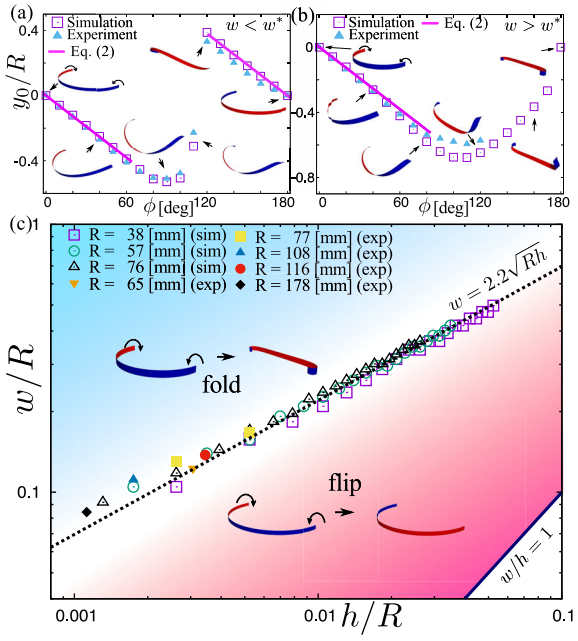

FIG. 3. (a),(b) Rescaled center position y_0/R plotted as a function of angle ϕ, for (a) a narrow ribbon with $(h, w, R) = (0.2, 8, 108)$ mm and for (b) a wide ribbon with $(h, w, R) = (0.2, 15, 108)$ mm. Open squares and filled triangles represent the simulation and experimental data, respectively. Snapshots are from our simulations. Solid lines denote our analytical prediction Eq. (2). (c) Transition-type diagram constructed from our experimental and numerical data for various combinations of (h, w, R). The dashed line represents the scaling prediction, Eq. (3): $w^*/R = 2.2\sqrt{h/R}$.

$y_0 \equiv y(s = 0)$ in Fig. 3(a). Initially, y_0 decreases linearly with ϕ and subsequently increases steeply just before the flip. For a wide ribbon with $w > w^*$, y_0 also decreases initially; however, it remains negative throughout the process [Fig. 3(b)]. Note that, during the simulation, we successfully reproduced the flip transition, where the shapes agree remarkably well with the experimental data [Fig. 1(c)]. The linear response can be understood analytically. In the linear elasticity theory, the elastic deformation energy is given by $E_{\rm rod} = \int ds(A_1\Omega_1^2 + A_2\Omega_2^2 + C\Omega_3^2)/2$ with the bending and twisting moduli given by $A_1 = Ehw^3/12$, $A_2 = Eh^3w/12$, and $C = Eh^3w/[6(1+\nu)]$. For our present purpose, it is useful to express Ω_a in terms of the Euler angles (φ, θ, ψ), where φ, θ, and ψ represent azimuthal, polar, and twist angles, respectively. This leads to $\Omega_1 = \varphi' \cos\theta \sin\psi - \theta' \cos\psi$, $\Omega_2 = \varphi' \cos\theta \cos\psi + \theta' \sin\psi$, and $\Omega_3 = \varphi' \sin\theta + \psi'$. To investigate the linear response, we expand the Euler angles around the base state of the semicircle: $\theta = \psi = 0$ and $\varphi' = 1/R$. Retaining the terms up to the quadratic orders in $E_{\rm rod}$ and taking the flat-ribbon limit $h/w \to 0$, we arrive at the Euler-Lagrange equations for ψ and θ as $\theta' = \psi/R$ and $\psi'''' - (\Gamma - 2)\psi''/R^2 + \psi/R^4 = 0$, where $\Gamma = (1+\nu)/2$. The equations can be solved for a general Γ [21]; however, the solutions are particularly compact for $\Gamma = 0$. We have $\psi(s) = -(2\phi/\pi)[(s/R)\sin(s/R) - \cos(s/R)]$. By integrating $\boldsymbol{r}'(s) = \hat{\boldsymbol{d}}_3$, the center line shape can be determined as

$$y_0 \simeq -\left(1 - \frac{2}{\pi}\right)\phi R. \tag{2}$$

This analytical prediction agrees remarkably well with our experimental and numerical results [solid lines in Figs. 3(a) and 3(b)] without fitting parameters. Equation (2) shows that the out-of-plane deflection y_0 arises owing to the coupling between the induced curvature $1/R$ and the twist ϕ. Note that Eq. (2) is also valid for the ribbon shape after the flip, with the replacement $\phi \to \phi - \pi$, as shown in Fig. 3(a).

Returning to Fig. 2(b), we note that the flip angle ϕ^* approaches 115° in the flat ribbon limit (for $\nu = 0.3$). The numerical simulations suggest that ϕ^* weakly depends on the Poisson ratio ν but falls into a narrow range from 110° ($\nu \simeq 0$) to 120° ($\nu \simeq 1/2$). We are currently unable to rationalize this observation by the Kirchhoff rod theory. For a complete theoretical understanding of Fig. 2(b), a stability analysis of a bent and twisted rod, as done for isotropic rods [42–44] and Möbius bands [40,45], will have to be developed for general anisotropic cross sections. We leave this theoretical challenge as a future subject and now proceed to determine the flip-fold phase boundary, using the result $\phi^* = 110°$–$120°$.

A mechanical equilibrium of a ribbon is determined by the energetic balance between bending and twisting [21,29]. Here, the twisting energy of a ribbonlike object consists of two parts, $E_{\rm twist} = E_{\rm Kirch} + E_{\rm str}$, where the former is the linear Kirchhoff strain energy over the thickness of the ribbon and the latter is from the in-plane stretch elasticity [26,27,29,46]. At equilibrium, for a given ϕ, $E_{\rm bend} \simeq E_{\rm twist}$ is expected, where $E_{\rm bend}$ is the ribbon's bending energy. Importantly, our numerical investigations suggest that a Kirchhoff rod (for which $E_{\rm str} = 0$) always undergoes a flip transition. Thus, if $E_{\rm Kirch} \gg E_{\rm str}$ and $E_{\rm Kirch} \simeq E_{\rm bend}$ are realized, the ribbon flips at ϕ^*, which is the case for a relatively narrow ribbon such that $w < w^*$. In contrast, for a sufficiently wide ribbon, the in-plane stretch elasticity contributes considerably to $E_{\rm twist}$. For $E_{\rm str} \simeq E_{\rm Kirch}$, a ribbon may behave more like a developable surface, for which a folding transition may occur. Thus, examining the relative significance of $E_{\rm Kirch}$ and $E_{\rm str}$ allows us to determine the boundary between the flipping and folding phenomena. Note that a typical twist is scaled as $\tau \simeq \phi/R$, and the Kirchhoff twist energy per length is given by $E_{\rm Kirch} = C\tau^2/2 \simeq Eh^3w\phi^2/[12(1+\nu)R^2]$. On the contrary, for a locally helicoidal midsurface, its Gaussian curvature is τ^2, which amounts to in-plane strain $\epsilon \simeq w^2\tau^2$. An exact analysis for a helicoid is shown to provide the stretching energy per length $E_{\rm str} = Ehw^5\phi^4/(1440R^4)$ [36,47]. A ribbon may flip for $E_{\rm bend} \simeq E_{\rm Kirch} > E_{\rm str}$ at $\phi \simeq \phi^*$, which predicts

$$w < w^* \simeq \left(\frac{120}{(1+\nu)\phi^{*2}}\right)^{1/4}\sqrt{Rh}. \tag{3}$$

For $\phi^* = 115°$ and $\nu = 0.3$, we predict $w^* \simeq 2.2\sqrt{Rh}$, which is in excellent agreement with our experiments and simulations including the prefactor [Fig. 3(c)], thus validating our physical argument. Note that the critical width w^* increases with the induced radius of curvature as $\sqrt{R}$ and weakly depends on the Poisson ratio.

When gravity dominates bending elasticity, the above results change significantly. The relative magnitude of gravity over elasticity is quantified by the dimensionless number R/ℓ_g, where $\ell_g = (Eh^2/12\rho g)^{1/3}$ is the gravito-bending length (with ρ the mass density of a rod) [48]. The limit of stiff rods or vanishing gravity corresponds to $R/\ell_g \to 0$. For the previously described metal ribbons and silicone rods, we estimate $\ell_g > 190$ mm and $\ell_g \simeq 33$ mm, which give $R/\ell_g = 0.1$–0.5 and $R/\ell_g \simeq 0.93$, respectively, justifying our earlier assumption. Alternatively, we test a ribbon made of PET, where we can realize the opposite regime $R/\ell_g > 1$ with $\ell_g \simeq 7.45 \pm 0.13$ cm. The most nontrivial behavior can be observed when an initial bending plane is set to be vertical [49]. Figure 4(a) shows ϕ^* obtained from the experiments and simulations as a function of R/ℓ_g. For $R/\ell_g < 1.13$, $\phi^* \simeq 115°$ even in the presence of gravity, again confirming the validity of our preceding analysis where $R/\ell_g \to 0$ was assumed. A novel morphology, termed the "M shape," appears for $R/\ell_g > 1.13$, at a stage prior to flipping [Figs. 4(a-i) and 4(a-ii)]. The ribbon's own weight stabilizes this concave shape, and an additional twisting is necessary to drive the system toward flipping instability [21]. Remarkably, ϕ^* increases discontinuously at $R/\ell_g \simeq 1.13$, suggesting that the nature of the transition alters in the presence of gravity. At approximately $R/\ell_g \simeq 1.4$, the M shape is stabilized further, and the flipping is no longer accessible even for $\phi = 180°$ [Figs. 4(a-iii) and 4(a-iv)]. Thus, the snaplike fast response should be explored for relatively narrow and stiff ribbons, satisfying $R/\ell_g < 1$.

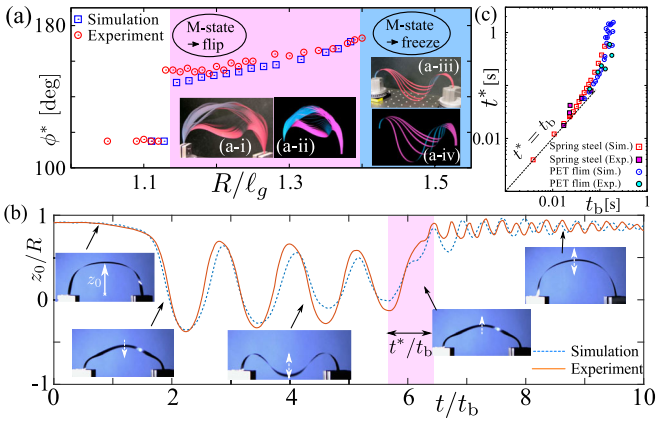

FIG. 4. (a) Flip transition angle ϕ^* plotted as a function of R/ℓ_g obtained from the simulations and experiments for polyethylene terephthalate (PET) ribbons with $(h, w) = (0.1, 4)$ mm. In the red region, the ribbon flips in the M-shaped configuration, while flipping is no longer observed in the blue region. (a-i) Experimentally and (a-ii) numerically obtained stroboscopic figures of a ribbon during flipping from a stable M-shaped configuration ($R/\ell_g \simeq 1.2$). (a-iii) Experimentally and (a-iv) numerically obtained stroboscopic figures of a ribbon that gets stuck in an M-shaped configuration ($R/\ell_g \simeq 1.5$). (b) Flip dynamics of a metal ribbon with $(h, w, R) = (0.2, 6, 66)$ mm. The solid and dashed lines represent the experimental and numerical time evolution, respectively, of the rescaled center position z_0/R. The red region defines the timescale of the flip t^*. (c) t^* obtained from the experiments and simulation is plotted as a function of t_b, with the dashed line $t^* = t_b$.

Note that there are a variety of shape transitions, i.e., flipping with and without the M shapes and folding and freezing in the M shape, under the influence of gravity. This implies that a precise control of the transitions may be possible with different external fields such as gravity, an electric field, and pressure. Even for a fixed ribbon geometry and materials, we may be able to control, store, and release the elastic energy of a constrained ribbon, by appropriately tuning an external force and twisting. Such rich morphological and responsive properties will be potentially advantageous for designing complex yet lightweight structures in the future.

Finally, we investigate the inertial dynamics by capturing the shape changes during the flip with a high-speed camera (Ditect, HAS-D71, 2000 fps). In Fig. 4(b) insets, we show a set of figures onset of flipping obtained from the experiment with $(h, w, R) = (0.2, 6, 66)$ mm. The video manifests that large-amplitude bending waves are excited when the head of the ribbon deflects downward and then moves upward with ringing. The characteristic frequency of the observed flexural wave may be determined by the growth rate of the most unstable mode. The linearized equation for an out-of-plane deflection u (in an appropriately defined coordinate) has a well-defined timescale $t_b = (2R)^2/hv_s$, where $v_s = \sqrt{E/\rho}$ is the speed of sound $v_s \equiv \sqrt{E/\rho}$ [10,50]. This arises as the frequency of the flexural wave [50] but also sets the growth timescale of unstable modes. In the main panel in Fig. 4(b), the numerically and experimentally obtained data for $z_0 \equiv z(s = 0)$ are plotted as a function of the rescaled time t/t_b, demonstrating that z_0 oscillates with the timescale of $t_b = 0.023$ s. We now define the flipping timescale t^* as indicated in Fig. 4(b). Figure 4(c) demonstrates that t^* is indeed of the order of t_b. A gradual departure from $t^* = t_b$ seen in Fig. 4(c) for larger $t_b \sim R^2$ suggests the weak system-size dependence. Critical slowing down could influence the overall flip dynamics for a long ribbon (i.e., for a larger R) [19].

In this study, we have investigated the qualitatively new snapping instability of a constrained ribbon and anisotropic rod by highlighting the prominent role of geometric twist-bend coupling. The results presented are generic and

scalable; thus they might be applied to a number of problems of different scales, from torsionally driven instability of DNA in nucleosomes [51,52] to the design of nonmuscular engines in soft robotics. It is an intriguing open question how the nature of the transition revealed here will be modified by thermal fluctuations, spontaneous curvatures, and/or active processes.

We acknowledge financial support in the form of Grants-in-Aid for Japan Society for the Promotion of Science (JSPS) Fellowship (Grant No. 16J05315) and JSPS KAKENHI (Grants No. 18K13519 and No. 18K18741).

*tomohiko.transfer@gmail.com
Present address: Flexible Structures Laboratory, Institute of Mechanical Engineering, École Polytechnique Fédérale de Lausanne, Lausanne, CH-1015, Switzerland.
†hwada@fc.ritsumei.ac.jp

[1] J. Dumais and Y. Forterre, Annu. Rev. Fluid Mech. **44**, 453 (2012).
[2] Y. Forterre, J. M. Skotheim, J. Dumais, and L. Mahadevan, Nature (London) **433**, 421 (2005).
[3] X. Noblin, N. O. Rojas, J. Westbrook, C. Llorens, M. Argentina, and J. Dumais, Science **335**, 1322 (2012).
[4] S. Armon, E. Efrati, R. Kupferman, and E. Sharon, Science **333**, 1726 (2011).
[5] H. Hofhuis, D. Moulton, T. Lessinnes, A.-L. Routier-Kierzkowska, R. J. Bomphrey, G. Mosca, H. Reinhardt, P. Sarchet, X. Gan, M. Tsiantis, Y. Ventikos, S. Walker, A. Goriely, R. Smith, and A. Hay, Cell **166**, 222 (2016).
[6] J. E. Gordon, *Structures: Or Why Things Don't Fall Down*, 2nd ed. (Da Capo Press, Cambridge, 2003).
[7] D. P. Holms and A. J. Crosby, Adv. Mater. **19**, 3589 (2007).
[8] D. Trivedi, C. D. Rahn, W. M. Kier, and I. D. Walker, Appl. Bionics Biomech. **5**, 99 (2008).
[9] E. Steltz, A. Mozeika, N. Rodenberg, E. Brown, and H. M. Jaeger, in *Proceedings of the 2009 IEEE/RSJ International Conference on Intelligent Robots and Systems* (IEEE, New York, 2009), pp. 5672–5677.
[10] A. Pandey, D. E. Moulton, D. Vella, and D. P. Holmes, Europhys. Lett. **105**, 24001 (2014).
[11] D. Bigoni, *Extremely Deformable Structures—CISM Lecture Notes No. 562* (Springer, New York, 2015).
[12] H. M. Jaeger, Soft Matter **11**, 12 (2015).
[13] D. Rus and M. T. Tolley, Nature (London) **521**, 467 (2015).
[14] P. M. Reis, J. Appl. Mech. **82**, 111001 (2015).
[15] P. M. Reis, H. M. Jaeger, and M. van Hecke, Ext. Mech. Lett. **5**, 25 (2015).
[16] Y. Morigaki, H. Wada, and Y. Tanaka, Phys. Rev. Lett. **117**, 198003 (2016).
[17] H. Yuk, S. Lin, C. Ma, M. Takaffoli, N. X. Fang, and X. Zhao, Nat. Commun. **8**, 14230 (2017).
[18] T. G. Sano and H. Wada, Phys. Rev. E **97**, 013002 (2018).
[19] M. Gomez, D. E. Moulton, and D. Vella, Nat. Phys. **13**, 142 (2017).
[20] T. Yu and J. A. Hanna, J. Mech. Phys. Solids **122**, 657 (2019).
[21] See Supplementary Material http://link.aps.org/supplemental/10.1103/PhysRevLett.122.114301 for movies and technical details, which includes Refs. [16,22–29].
[22] M. Sadowsky, Sitzungsberichte der Königlich Preußischen Akademie der Wissenschaften zu Berlin **22**, 412 (1930).
[23] M. Sadowsky, *Verhandl. Des 3. Intern. Kongr. f. Techn. Mechanik, 1930, Teil II*, edited by A. C. W. Oseen and W. Weibull (AB Sveriges Litografiska Tryckerier, 1931), p. 444.
[24] G. Chirico and J. Langowski, Biopolymers **34**, 415 (1994).
[25] G. Chirico, Biopolymers **38**, 801 (1996).
[26] R. Ghafouri and R. Bruinsma, Phys. Rev. Lett. **94**, 138101 (2005).
[27] D. Grossman, E. Sharon, and H. Diamant, Phys. Rev. Lett. **116**, 258105 (2016).
[28] T. R. Powers, Rev. Mod. Phys. **82**, 1607 (2010).
[29] B. Audoly and Y. Pomeau, *Elasticity and Geometry* (Oxford University Press, New York, 2010).
[30] A. Yamada, H. Mameda, H. Mochiyama, and H. Fujimoto, in *Proceedings of the 2010 IEEE/RSJ International Conference on Intelligent Robots and Systems* (IEEE, New York, 2010), pp. 389–394.
[31] N. Fukamachi and H. Mochiyama, in *Proceedings of the 2015 IEEE International Conference on Advanced Intelligent Mechatronics (AIM)* (IEEE, New York, 2015), p. 1102.
[32] Y. Sugiyama and S. Hirai, Int. J. Robotics Res. **25**, 603 (2006).
[33] J. D. Moroz and P. Nelson, Macromolecules **31**, 6333 (1998).
[34] R. E. Goldstein, T. R. Powers, and C. H. Wiggins, Phys. Rev. Lett. **80**, 5232 (1998).
[35] J. Chopin and A. Kudrolli, Phys. Rev. Lett. **111**, 174302 (2013).
[36] J. Chopin, V. Démery, and B. Davidovitch, J. Elast. **119**, 137 (2015).
[37] M. A. Dias and B. Audoly, J. Elast. **119**, 49 (2015).
[38] Z. Shen, J. Huang, W. Chen, and H. Bao, Comput. Graph. Forum **34**, 145 (2015).
[39] G. H. M. van der Heijden and J. M. T. Thompson, Physica (Amsterdam) **112D**, 201 (1998).
[40] E. L. Starostin and G. H. M. van der Heijden, Nat. Mater. **6**, 563 (2007).
[41] J. Chopin and A. Kudrolli, Soft Matter **12**, 4457 (2016).
[42] J. H. Michell, Mess. Math. **11**, 181 (1890).
[43] E. E. Zajac, J. Appl. Mech. **29**, 136 (1962).
[44] A. Goriely, J. Elast. **84**, 281 (2006).
[45] L. Mahadevan and J. B. Keller, Proc. R. Soc. A **440**, 149 (1993).
[46] S. Armon, H. Aharoni, M. Moshe, and E. Sharon, Soft Matter **10**, 2733 (2014).
[47] A. E. Green, Proc. R. Soc. A **161**, 197 (1937).
[48] C. Wang, Int. J. Mech. Sci. **28**, 549 (1986).
[49] If an initial bending plane is horizontal, gravity may act to impede flipping when it first moves downward upon twisting. In the same configuration, when the ribbon initially moves upward (i.e., by twisting it in the opposite direction), gravity may work to assist flipping. The effects of gravity in these two cases are thus easy to understand.
[50] B. Audoly and S. Neukirch, Phys. Rev. Lett. **95**, 095505 (2005).
[51] C. Lavelle, Biochimie **89**, 516 (2007).
[52] F. Kouzine, A. Gupta, L. Baranello, D. Wojtowicz, K. Ben-Aissa, J. Liu, T. M. Przytycka, and D. Levens, Nat. Struct. Mol. Biol. **20**, 396 (2013).